Kidney International, Vol. 43 (1993), pp. 334–345

Renal basement membranes by ultrahigh resolution scanning electron microscopy

KAZUE HIRONAKA, HIROFUMI MAKINO, YASUSHI YAMASAKI, and ZENSUKE OTA

Third Department of Internal Medicine, Okayama University Medical School, Okayama, Japan

Renal basement membranes by ultrahigh resolution scanning electron microscopy. Three-dimensional ultrastructures of basement membranes of the rat kidney were investigated with an ultrahigh resolution scanning electron microscope (HSEM) equipped with a resolving power of 0.5 nm. All cellular components were extracted from renal cortical tissues by sequential-detergent treatment. Four types of acellular basement membranes were observed after tannin-osmium conductive staining: the glomerular basement membrane (GBM) associated with the mesangial matrix, the tubular basement membrane (TBM), the Bowman's capsule basement membrane (BCBM), and the peritubular capillary basement membrane (PTCBM). We could demonstrate the polygonal meshwork structures composed of strands in the respective basement membranes. The strands averaged 6 to 7 nm wide, whereas the pore sizes within the meshworks were variable and differed according to the basement membrane type. Moreover, we confirmed the presence of the heterogeneity of the GBM suggested by several approaches. Present data support the proposition that a polygonal meshwork structure may represent the basic structure of basement membrane. Some of the observed architectural dissimilarities in basement membrane types may reflect their different functional properties, which in turn may reflect the heterogeneous distribution of major basement membrane components as demonstrated by immunohistochemical and biochemical studies.

The glomerular basement membrane (GBM) is physiologically and morphologically best studied in relation to glomerular permselectivity of macromolecules and plasma protein in normal and diseased glomeruli. Physiological studies have proved that the GBM constitutes both the size-selective and the charge-selective barrier, and are suggestive of the presence of the pores in the GBM [1–7]. Type IV collagen is considered to play an important role in the size-selective permeability of the GBM. More recently, the GBM is considered to contain at least five distinct type IV collagen chains: α1(IV), α2(IV), α3(IV), α4(IV) and α5(IV) [8–20]. Immunohistochemical and biochemical studies suggest that novel chains designated as α3, α4, and α5 may have a crucial role in glomerular filtration function. At the level of ultrastructure, the GBM has usually been described as a thin layer composed of fibrillar networks of 3 to 4 nm fibrils [1]. The presence of the pores in the network of the GBM have been demonstrated with transmission electron microscopy (TEM) of ultrathin section method [21], negative staining [22, 23], and replica method [24] without proteolytic digestion. However, ultrastructural features of the GBM vary with the method employed. This is in part due to the difficulty in preparation for the GBM for ultrastructural analysis.

Scanning electron microscope (SEM) has the advantage over TEM in that it can observe wide surfaces three-dimensionally. However, application of SEM has previously been limited to glomerular cell surfaces, because the GBM underlies epithelial and endothelial cells. A nondisruptive technique for acellular preparation of renal cortex was devised by Carlson and Kenny [25]. This method has made possible meaningful morphological investigation of the isolated GBMs [26–30]. Nevertheless, previous SEM studies failed to demonstrate the network structure of the GBM, probably due to (1) the insufficient instrument resolving power (about 5 nm or larger), and (2) problems with the metal coating used to increase electron-conductivity of biological specimens. First, a new type SEM, that is, ultrahigh resolution scanning electron microscopy (HSEM) was devised by Tanaka et al in 1985 [31]. HSEM is equipped with a field emission source and objective lens of very short focal length, and a resolving power of 0.5 nm at 30 kV. Therefore, HSEM theoretically enables imaging biological specimens up to macromolecular architecture, if they are appropriately prepared. Second, the metal coating is inadequate for ultrastructural observation, because metal particles, being generally larger than the resolution of the HSEM, appear as pebbles or granular objects which distort the image of the macromolecules. The tannin-osmium conductive staining originally devised by Murakami [32], which is the one of the methods used to increase electron-conductivity of the biological specimens, is widely employed in ultrastructural studies using HSEM [33–35].

The purpose of the present HSEM study is to extend the previous SEM studies up to the level of macromolecular resolution, and demonstrate some general and specific ultrastructural features of basement membrane types. After extraction by the Carlson method [25], four types of acellular basement membranes were examined by HSEM and TEM: the GBM associated with the mesangial matrix, the tubular basement membrane (TBM), the Bowman's capsule basement membrane (BCBM), and peritubular capillary basement membrane (PTCBM). We carried out TEM studies mainly to judge the morphological integrity of isolated basement membranes. We could demonstrate polygonal meshwork structures composed of strands about 6 to 7 nm wide and pores in all basement membranes using HSEM in conjunction with tannin-osmium conductive staining.

Received for publication March 3, 1992
and in revised form August 24, 1992
Accepted for publication August 24, 1992

Methods

Ten male Wistar rats, weighing approximately 200 g were used for the experiments. After anesthetization with ether, kidneys were extracted immediately.

Preparation of acellular renal cortex

Acellular cortical tissues were prepared as previously described [29, 30]. Briefly, renal cortical tissue blocks were minced to 2 mm^3. Minced tissue specimens were sequentially exposed to 4 mM ethylenediamine tetraacetic acid (24 hr, 4°C), 3% triton X-100 (24 hr, 4°C), 0.05% deoxyribonuclease (Type I, Sigma, St. Louis, Missouri, USA) in 1 M NaCl (24 hr, 4°C), and 4% sodium deoxycholate (2 to 4 hr, room temperature). All solutions contained 0.1% sodium azide. Tissue specimens were rinsed extensively between each step with distilled water. Acellular renal cortical specimens were separated for HSEM and TEM preparation.

Tissue preparation for HSEM

Acellular renal cortical specimens were prepared for HSEM as previously described [33]. Briefly, specimens were fixed with 2.5% glutaraldehyde in 0.1 M cacodylate buffer (pH 7.2, 2 hr, 4°C). After rinsing with the same buffer, the tannin-osmium conductive staining (OTOTO method) was performed as follows: by immersion three times in 1% osmium tetroxide (2 hr, 4°C), and interposed by 2% tannic acid solution (pH 4.2, 2 hr, room temperature). Between each step, rinses were performed at least three times with distilled water. After staining, specimens were dehydrated in graded series of ethanol and cryofractured in liquid nitrogen. Cryofractured specimens were transferred to t-buty alcohol, and freeze-dried with a vacuum evaporator (ID-2, Eiko). The dried specimens were then mounted on aluminum stubs, and examined with an ultrahigh resolution scanning electron microscope (S-900, Hitachi) without metal coating at original magnifications 250 to 600,000× using an accelerating voltage of 20 kV.

Tissue preparation for TEM

Acellular renal cortical specimens were immersed into 2.5% glutaraldehyde in 0.1 M cacodylate buffer (pH 7.2, 2 hr, 4°C), postfixed in 1% osmium tetroxide (2 hr, 4°C), and then embedded in Epon after dehydration in graded series of ethanol. Thin sections were stained with uranyl acetate and lead citrate and examined with a transmission electron microscope (H-700, Hitachi) at 75 kV. Some of the specimens, followed by the tannin-osmium staining, were observed with TEM without uranyl acetate and lead citrate staining.

Morphometric analysis

HSEM micrographs were selected for measurements when meshwork structures were observed *en face* view at higher magnifications in order to tend to "flatten" the basement membrane surface and to reduce secondary errors caused by its waviness. Measurements of the meshworks composed of strands and pores were made on HSEM micrographs with an original magnification of 200,000×. The long dimension of the pores and the perpendicular width of the strands were measured by an ocular micrometer equipped with a 0.1 mm scale. Mean value and standard deviation were determined.

Results

Following cell solubilization in minced renal cortical tissues, all cellular components were completely removed and only basement membranes, the mesangial matrix, and interstitial collagen fibers remained with *in vivo* architectures (Figs. 1 A–D, 2A). Acellular renal cortical tissues were judged by TEM to consist of intact basement membranes devoid of attached cellular components before and after tannin-osmium staining (Fig. 1 C, D).

Glomerular basement membrane

At low magnification HSEM (Fig. 2 A, B), peripheral loops of GBMs were cryofractured in various sectioned planes and maintained their intrinsically lobulated architecture without support from glomerular cells. The mesangial matrix extended from the centrolobular zone onto the endothelial side of the peripheral GBM for variable distances (Fig. 1B, 2C, arrows). The epithelial surface of the GBM was smooth in peripherally expanded areas (Fig. 2B, Ep), although it was often wrinkled and occasionally pitted in juxtamesangial areas (Fig. 2B, arrowheads). In contrast, the endothelial side of the GBM was much more irregular, especially close to the centrolobular zone (Fig. 2B, thick arrows), where the mesangial matrix showed a fenestrated septum with round or oval stomata between adjacent glomerular channels. At higher magnification HSEM (Fig. 2C), the mesangial fenestrated septum showed a plexus composed of intertwining long fibrils. The isolated GBM was about 110 to 170 nm thick in the perpendicularly fractured face (Fig. 2D). It appeared to consist of a densely packed amorphous materials and pores about 10 nm in diameter seen in places (Fig. 2D, arrows). By TEM, the fibrillar components of the GBM embedding in background amorphous materials were about 3 to 4 nm wide in conversional TEM preparation (cf. Fig. 1C) and 4 to 6 nm wide after tannin-osmium conductive staining (cf. Fig. 1D) at much higher magnification.

At higher magnification HSEM (Fig. 3A), the mesangial matrix extending onto the endothelial surface of the GBM appeared as a series of anastomosing ridges. The strands extending from the ridges were distributed in a polygonal array and formed a specific endothelio-mesangial surface of the GBM (Fig. 3B). It appeared to consist of an irregular, loose meshwork structure of strands about 6 nm wide and pores that ranged from 4 to 120 nm with an average 14.1 nm in diameter (cf. Fig. 9 A, B). Some of the strands were in direct continuity with the intrinsic meshwork structure of the GBM (Fig. 3B, arrowheads).

On the endothelial surface of the peripheral GBM (Fig. 3 C, D), the mesangial expansion was scarce or absent, where the meshwork structure of the GBM was more clearly imaged in oblique than in *en face* view (Fig. 3D). The strands and pores within the meshworks averaged 6.4 nm wide and 9.7 nm in diameter, respectively (cf. Fig. 10 A, B).

The epithelial surface of the GBM showed a more polymeric meshwork structure composed of strands that frequently ascended or descended from one plane to the next (Fig. 3 E, F). Each strand (about 6 nm wide) joined to three or four other strands. The strands had relatively smooth surfaces, but further detail on these features failed to be clarified even at much higher magnifications (Fig. 3F, arrowheads). The pores within the

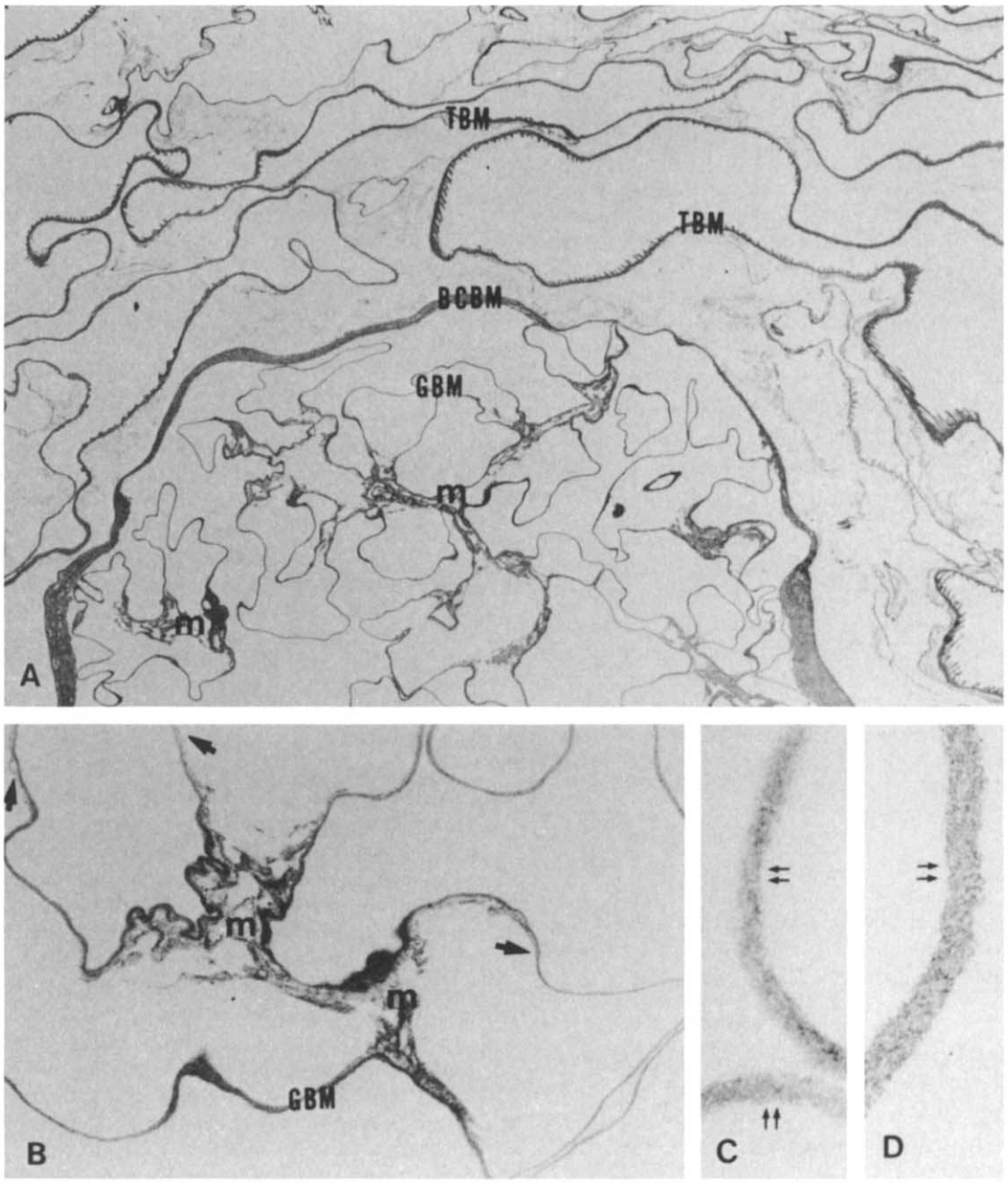

Fig. 1. *Transmission electron micrographs (TEM) of rat acellular renal cortex prepared by sequential-detergent treatment.* **A.** All cellular components were completely removed. Glomerular basement membranes (GBMs) associated with the mesangial matrix (m), Bowman's capsule basement membranes (BCBMs), tubular basement membranes (TBMs), peritubular capillary basement membranes, and interstitial collagen fibers remained. ×1,400. **B.** The mesangial matrix (m) extends from the centrolobular zone to the endothelial surface of the peripheral GBMs (arrows). ×6,000. Acellular GBM conventionally prepared (**C**) and after tannin-osmium conductive staining (**D**). Double arrows indicate endothelial surface of the GBM. Overlying cell layers were completely removed. ×44,000.

meshwork were oval or polygonal and varied in size, ranging from 4 to 20 nm with an average of 9.7 nm in diameter (cf. Fig. 11 A, B). Knob-like granular materials (about 15 nm wide) were occasionally observed on both sides of the GBM (Fig. 3F, asterisk).

Bowman's capsule basement membrane

The Bowman's capsule basement membrane (BCBM) was the thickest basement membrane among the four renal basement membranes. In cross section (Fig. 4 A, B, C), the perpendicularly fractured face displayed a multilayered structure. Between each layer, strands running mainly in one direction formed loose meshworks that ranged from 4 to 50 nm in diameter (Fig. 4C, arrows). The epithelial surface of the BCBM showed a corrugated appearance (Fig. 2A, 4D). At higher magnification (Fig. 4E) an irregular meshwork structure composed of strands was observed. Strands were about 7 nm wide and pores within the meshworks varied from 3 to 42 nm with an

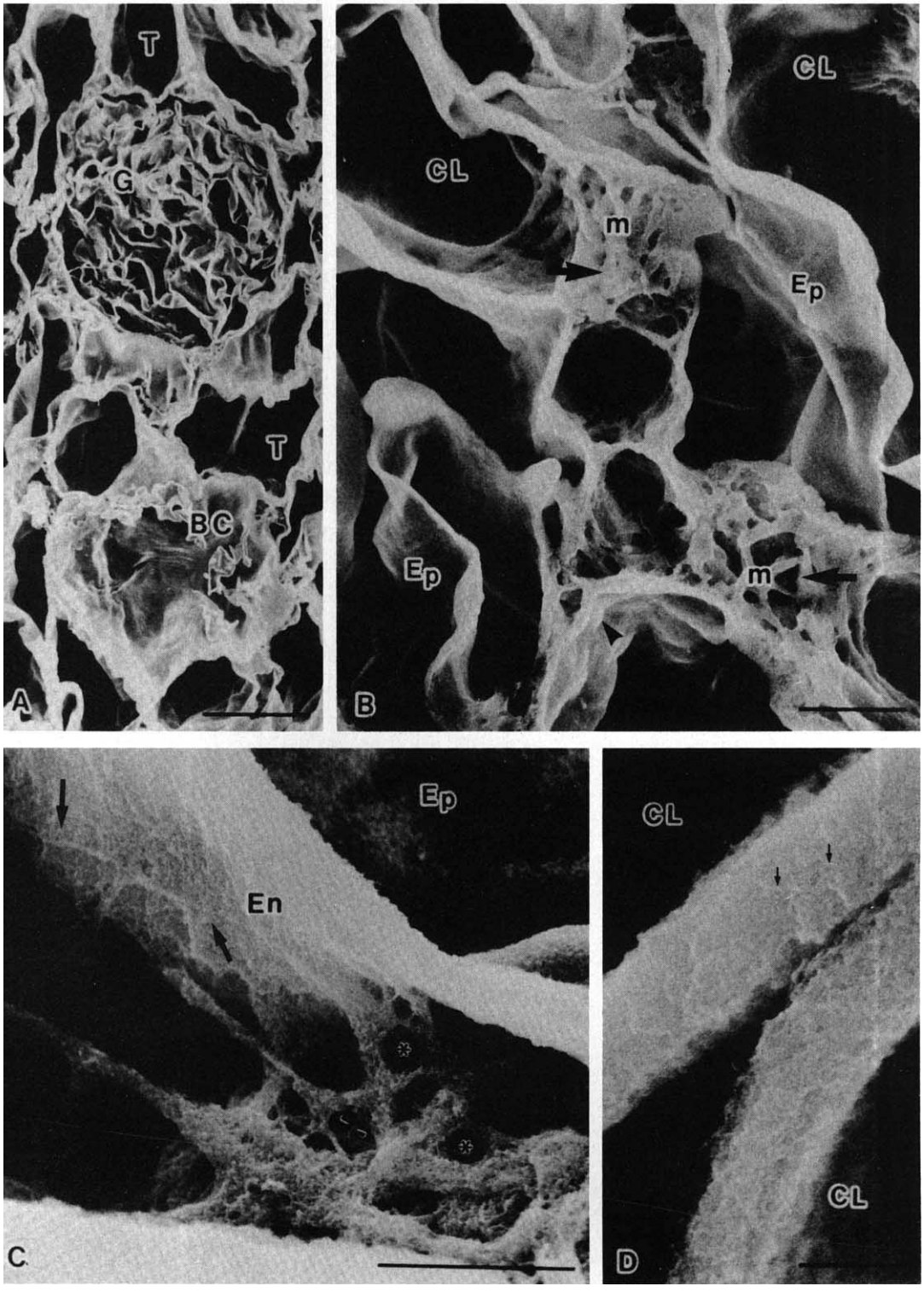

Fig. 2. *Ultrahigh resolution scanning electron micrographs (HSEM) of detergent-treated renal cortex.* **A.** HSEM of cryofractured acellular renal cortex showing a glomerular tuft (G) and an empty Bowman's capsule (B) with tubules (T) devoid of overlying cell layers. ×700, bar = 30 μm. **B.** Epithelial surfaces (Ep) of the acellular GBM of are smooth, but in juxtamesangial areas often wrinkled and pitted (arrowheads). Endothelial surfaces are irregular in the centrolobular zones (thick arrows), where the mesangial matrix (m) appears as a fenestrated septum with round or oval stomata. CL: capillary lumen, ×6,600, bar = 3 μm. **C.** Higher magnification of the mesangial matrix (m) composed of intertwining fine fibrils (arrowheads) in the centrolobular zone. Asterisks indicate round or oval stomata of the mesangial fenestrated septum. Arrows indicate the mesangial matrix extending onto the endothelial surfaces (En). ×24,000, bar = 1.5 μm. **D.** The perpendicularly fractured face of the peripheral GBM. Note small pores (arrows). ×132,000, bar = 150 nm.

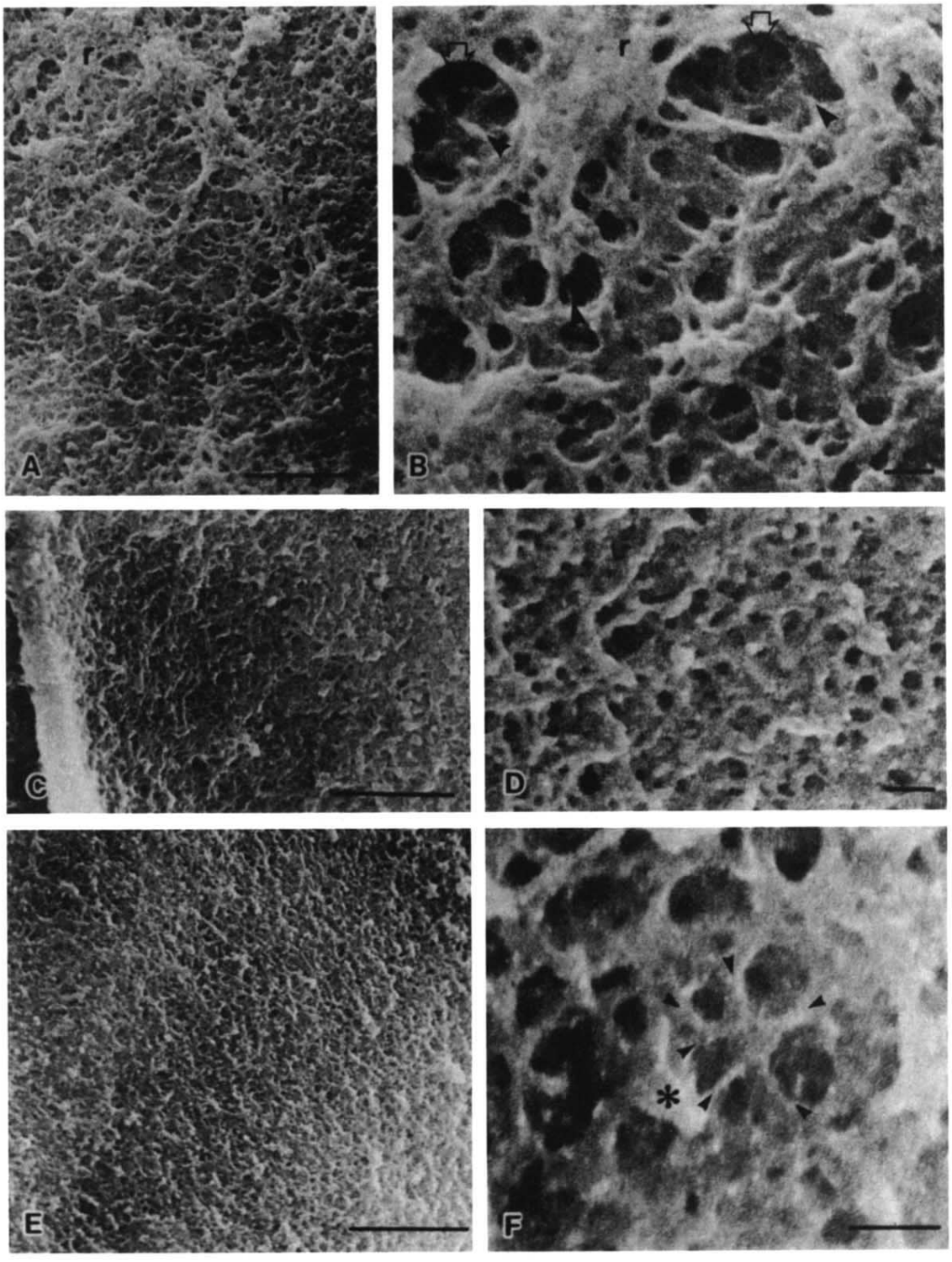

Fig. 3. *Meshwork structures of the GBM on the endothelio-mesangial surface (A, B), the endothelial surface (C, D), and the epithelial surface (E, F).* **A.** The mesangial matrix appears as a series of anastomosing ridges (r) on the endotheliomesangial surface. ×66,000, bar = 300 nm. **B.** Higher magnification of the area similar to that in **A** showing a loose, polygonal meshwork structure composed of 6 nm wide strands. Thin arrows indicate the long dimension of pores of meshworks. Some of the strands (arrowheads) are directly connected with the GBM (open arrows). ×264,000, bar = 30 nm. **C.** The mesangial matrix is absent on the endothelial surface of the peripheral GBM. ×66,000, bar = 300 nm. **D.** Higher magnification of the area similar to that in **C** showing a meshwork structure composed of strands and pores. ×264,000, bar = 30 nm. **E.** The epithelial surface showing a polymeric meshwork structure composed of strands. ×66,000, bar = 300 nm. **F.** Strands about 6 nm wide (arrowheads) have relatively smooth surfaces. Note knob-like granular materials (asterisk). ×540,000, bar = 30 nm.

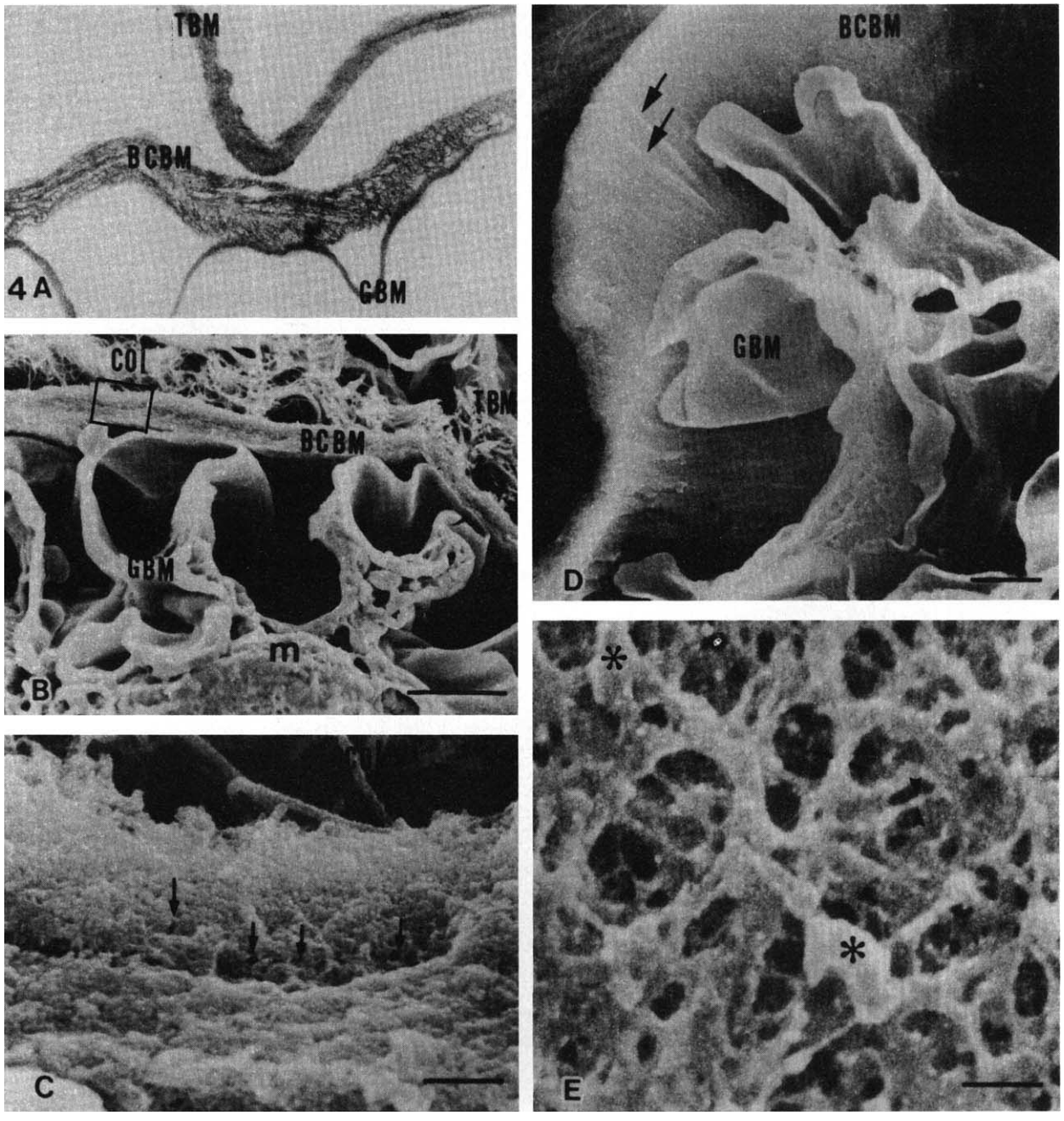

Fig. 4. *Acellular Bowman's capsule basement membrane (BCBM).* **A, B** and **C** show a multilayered structure of the BCBM. GBM: glomerular basement membrane. TBM: tubular basement membrane, col: interstitial collagen fibers, m: mesangial matrix. (**A,** ×6,600, **B,** ×4,800, bar = 3 μm). **C.** Details of the area in the rectangle in **B** showing pores (about 4 to 50 nm, arrows) between each layers. ×40,000, bar = 300 nm. **D.** The epithelial surface of the BCBM reveals a corrugated appearance (arrows). ×3,800, bar = 3 μm. **E.** Higher magnification of the area similar to that in **D** showing an irregular meshwork structure composed of strands (arrowheads). Asterisks indicate scattered knob-like granular materials. ×400,000, bar = 30 nm.

average of 14.1 nm in diameter (cf. Fig. 12 A, B). The overall structure was closely similar to that of the luminal surface of the TBM (cf. Fig. 7 A, B).

Peritubular capillary basement membrane

The peritubular capillary basement membrane (PTCBM) was the thinnest of the renal basement membranes (Fig. 5A, asterisks) and the epithelial surface showed a meshwork structure (Fig. 5B). Interstitial collagen fibers were identified between the TBM and the PTCBM (Fig. 5B, col).

Tubular basement membrane

Tubular basement membranes (TBMs) averaged threefold in thickness as compared with GBMs (Fig. 4A). Proximal TBMs were distinguished by specific dentate evaginations extending into the tubular lumen (Fig. 6A, arrows), which corresponded

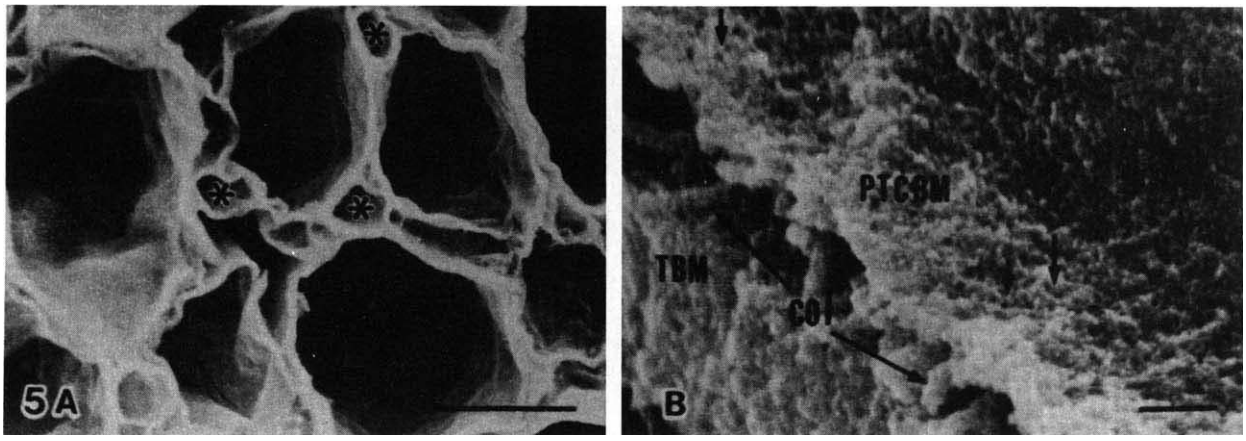

Fig. 5. *A. HSEM of cross-sectioned acellular tubules (T) and acellular peritubular capillaries (asterisks).* ×1,300, bar = 15 μm. **B.** Peritubular capillary basement membrane (PTCBM) is separated from the tubular basement membrane (TBM) by interstitial collagen fibers (col). Note small pores (arrows) on the epithelial surface of the PTCBM. ×66,000, bar = 150 nm.

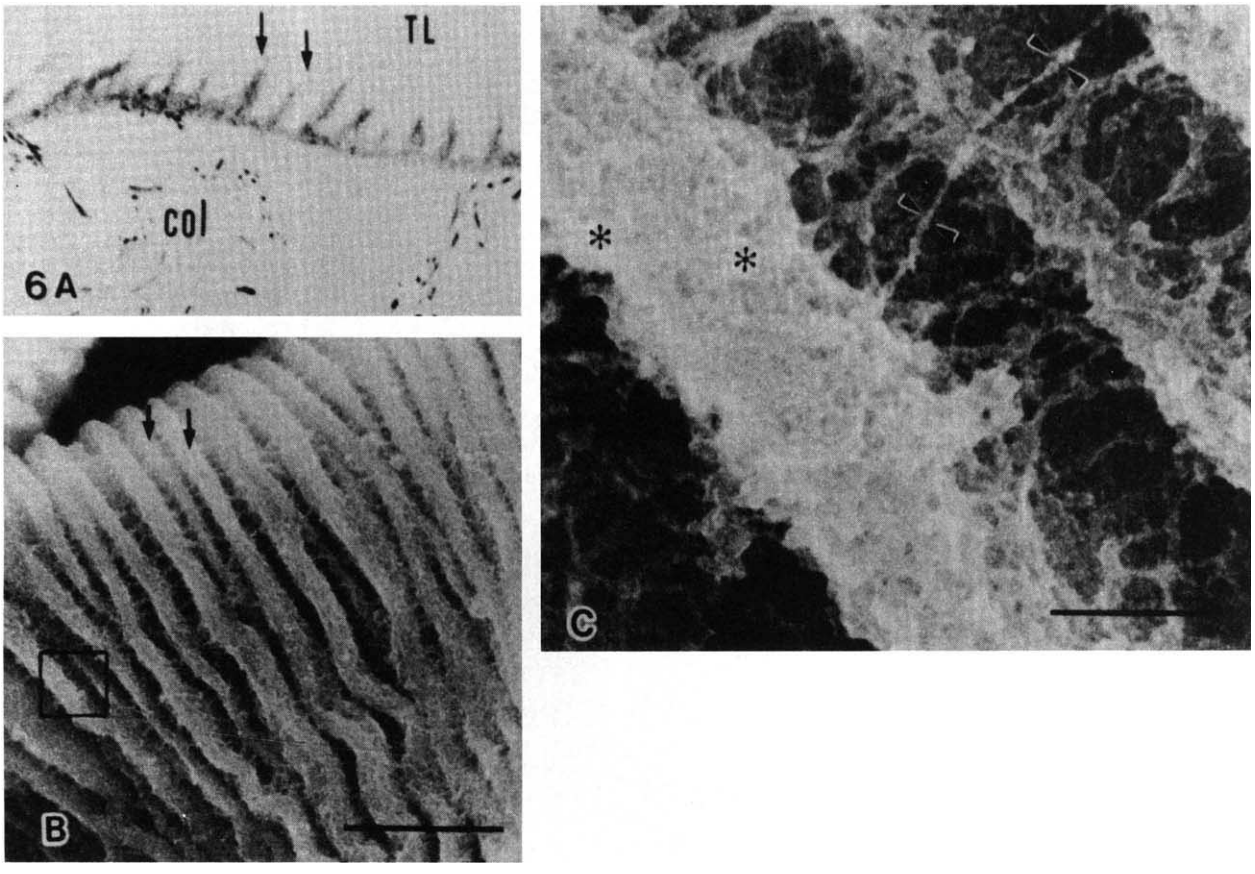

Fig. 6. *Acellular basement membrane of proximal tubule (pTBM).* **A.** TEM showing dentate evaginations (arrows) of the pTBM into the tubular lumen (TL). ×10,000. **B.** HSEM showing many parallel cristae (arrows) on the epithelial surface of the pTBM. ×13,000, bar = 1.5 μm. **C.** Details of the area shown in the rectangle in **B.** Arrowheads indicate long fibrillar components between each crista. Note scattered amorphous granular materials (asterisks) on the crista. ×132,000, bar = 150 nm.

to many parallel cristae on ultrahigh scanning electron micrographs (Fig. 6B, arrows). At higher magnification HSEM (Fig. 6C), the epithelial surface of the proximal TBM showed a specific, loose meshwork structure in the invaginated portions between each crista. The loose meshwork structure consisted of strands about 7 nm wide and 4 to 100 nm long (Fig. 6C, arrowheads). On the other hand, a tight meshwork structure with amorphous granular materials was observed on the crista (Fig. 6C, asterisks).

In the more distal segments of the renal tubules, the epithelial

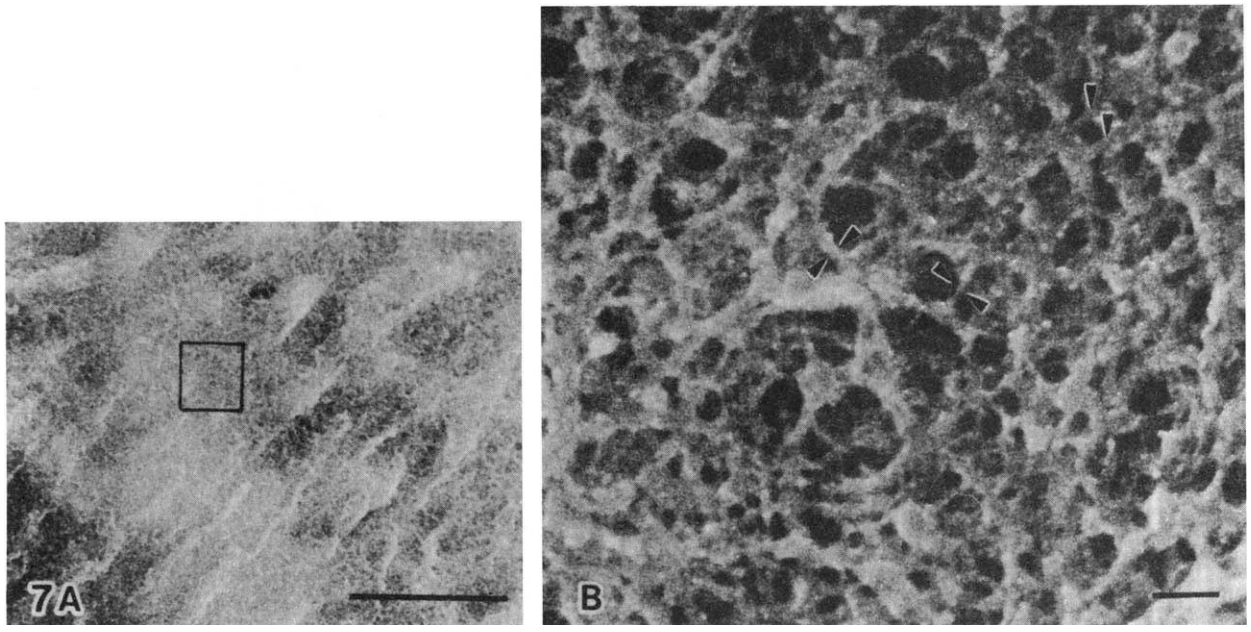

Fig. 7. *Acellular basement membrane of distal tubule (dTBM).* **A.** The epithelial surface reveals a less corrugated appearance. **B.** Details of the area in the rectangle in **A** showing a polygonal meshwork structure composed of strands (arrowheads) and pores. ×264,000, bar = 30 nm.

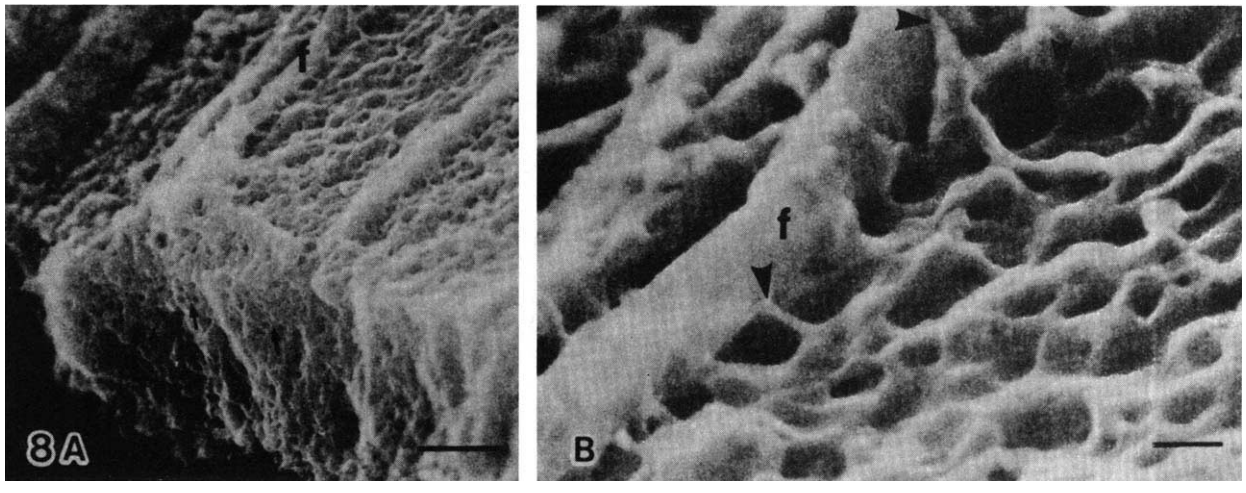

Fig. 8. *Meshwork structures of the interstitial surface of tubular basement membrane (TBM).* **A.** Note small pores (arrows) in perpendicularly fractured face. f: interstitial collagen fiber, ×66,000, bar = 150 nm. **B.** Higher magnification of the area similar to that in **A** showing an irregular meshwork structure. Thick fibers (50 nm wide, f) are directly connected (arrowheads) with the TBM. ×288,000, bar = 30 nm.

surface of the TBM had a less corrugated appearance (Fig. 7A), where an irregular meshwork structure was observed without the specific patterns seen in the proximal TBM (Fig. 7B). The strands and pore size within the meshworks averaged 6.8 nm wide and 13.1 nm in diameter, respectively (cf. Fig. 13A, B).

The interstitial surface of the TBM showed an irregular meshwork structure (Fig. 8 A, B). The strands and pores within the meshworks averaged 6.9 nm wide and 13.5 nm in diameter, respectively (cf. Fig. 14 A, B). Pores were also observed in the perpendicularly fractured face (Fig. 8A, arrows). Thick fibers (~50 nm wide) which tended to be arranged perpendicularly to the longitudinal axis of tubules, were directly connected (Fig. 8B, arrowheads) with the TBM in places.

Figures 9 through 14 indicate the distribution of width of the strands (A) and diameter of the pores (B) measured in the meshwork structures of the GBM (Figs. 9–11), BCBM (Fig. 12) and TBMs (Figs. 13, 14), respectively.

Discussion

Technique for ultrastructural analysis

In this study, we investigated *in situ* ultrastructural features of renal basement membranes using HSEM. HSEM is a new technique that has proven its value in revealing novel features of glomerular components [33–35]. Using this new technique, we have previously demonstrated the presence of the pores in

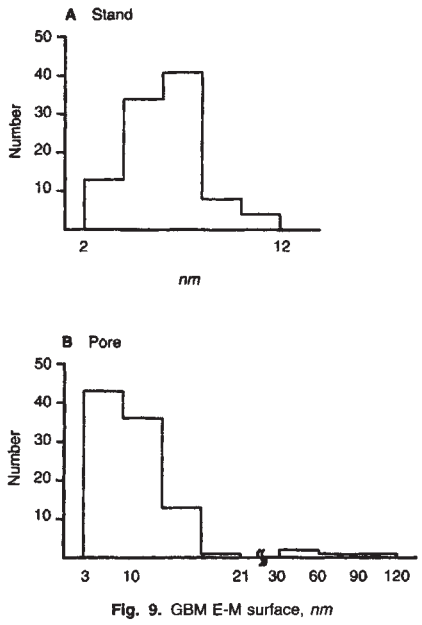

Fig. 9. GBM E-M surface, *nm*

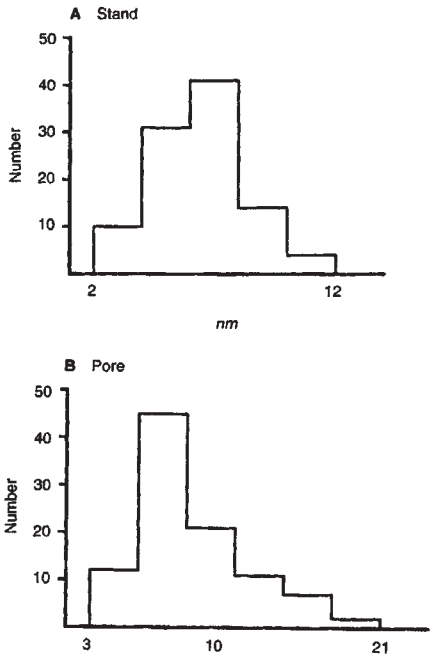

Fig. 10. GBM En surface, *nm*

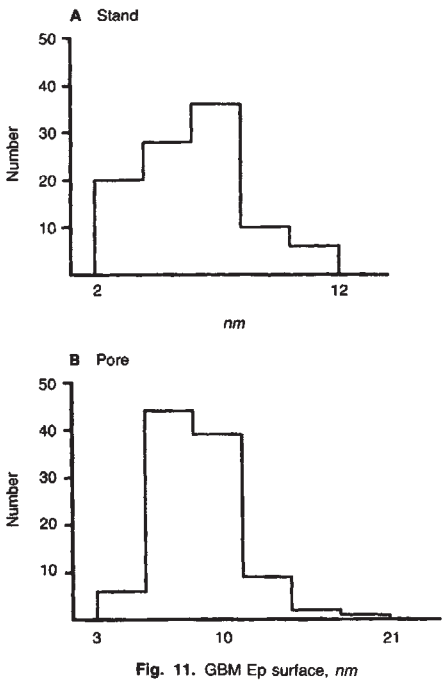

Fig. 11. GBM Ep surface, *nm*

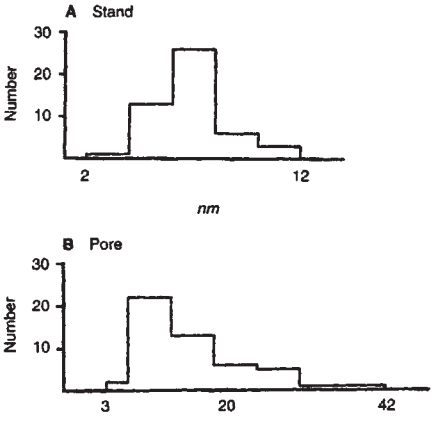

Fig. 12. BCBM Ep surface, *nm*

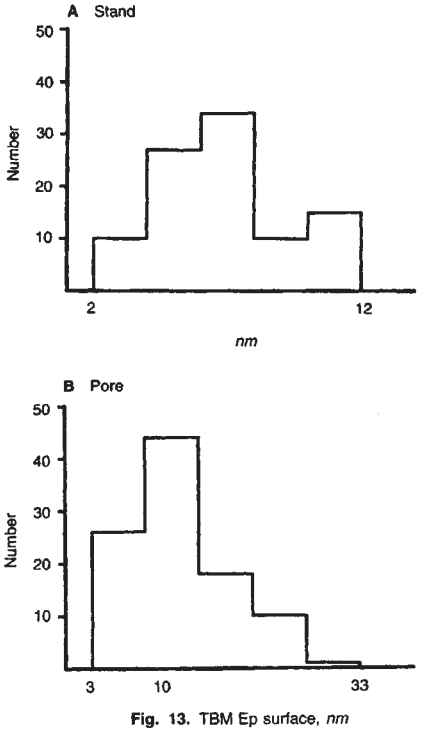

Fig. 13. TBM Ep surface, *nm*

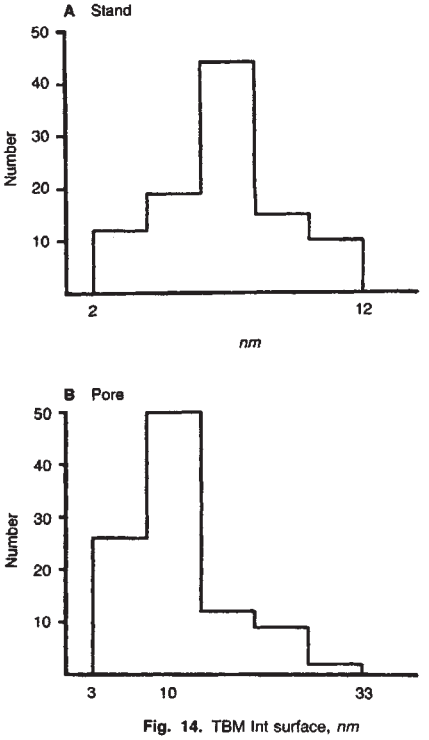

Fig. 14. TBM Int surface, *nm*

Figs. 9 to 14. *Histograms of the distribution of width of the strands (A) and diameter of the pores (B) measured from the meshwork structure in the GBM (Figs. 9–11), the BCBM (Fig. 12), and the TBM (Figs. 13, 14).* E-M surface: endothelio-mesangial surface, En surface: endothelial surface, Ep surface: epithelial surface, Int surface: interstitial surface.

the meshwork structure of the rat GBMs prepared by sonication method [33]. The Carlson extraction method [25] has the advantage over the Spiro sonication method [36]. Namely, it yields a completely acellular preparation of renal cortex, the extracellular matrix of which maintains its *in vivo* architecture and allows clear determination of the surface of the basement membrane observed. The integrity of detergent-treated basement membranes has been proven in several approaches [29,

37–39]. We confirmed that renal cortical tissues extracted by this method consist of intact basement membranes devoid of overlying cell layers by TEM and HSEM. Consequently, we could demonstrate the previously unrecognized meshwork structures by conventional SEM studies on basement membrane types.

Meshwork structures in basement membrane types

The open, lobulated profiles of acellular GBMs suggest an intrinsic structural rigidity unrelated to support by glomerular cells and stretching by the hydraulic pressure *in situ*. On the epithelial surface pitted holes were observed, which were in agreement with previous reports [26], but their function is unknown. The corrugated appearances in the TBM and BCBM may represent manifestations of increased mechanical stress *in situ*.

At higher magnifications, respective basement membranes appeared to be mainly composed of 6 to 7 nm wide strands arranged in polygonal meshworks, and to a lesser extent granular materials. The pore sizes of the meshworks were different among basement types. The pore sizes averaged 9.7 nm, 14.1 nm, and 13.1 nm in diameter in the epithelial surface of the GBM, BCBM, and TBM, respectively (cf. Fig. 11B, 12B, 13B). The pore size characterizing the epithelial surface of the GBM was smaller than in other basement membranes. Similar conclusions was described by other investigators [21, 40, 41]. Laurie et al have demonstrated in the anastomosing network of 4 to 5 nm wide "cords" the presence of the pores that ranged from 8 to 15 nm, in the GBM [21], thin basement membranes [40], and the surface of Reichert's membrane [41] by TEM of ultrathin section technique.

Present data support the proposition that a polygonal meshwork structure may represent a basic, ultrastructural feature of basement membranes [40–42]. The ultrastructural dissimilarities observed in renal basement membrane types may reflect the differences in the distribution and in the relative amounts of major basement membrane components such as type IV collagen, laminin, heparan sulfate proteoglycan and entactin demonstrated in immunohistochemical and biochemical studies [19, 21, 43–49]. These biochemical and structural dissimilarities may relate to the diverse physiological roles in basement membrane types. More recently, renal basement membranes are believed to contain at least five distinct type IV collagen chains: α1(IV), α2(IV), α3(IV), α4(IV), and α5(IV) [8–20]. Heterogeneous distributions of them in basement membrane types have been demonstrated and the α5(IV) chain is considered to be almost completely restricted to the GBM [16]. Those immunohistochemical and biochemical studies suggest that novel chains designated as α3, α4, and α5 may have a crucial role in glomerular filtration function, however, differences in function among the various α-chains have not yet been determined.

Meshwork structure of GBM

In general, the GBM has been described to consist of the network of 3 to 4 nm fibrils [1]. Laurie et al [21] have designated the 4 nm wide fibrils as "cords". Ota et al [22] and Martinez-Hernandez [23] have demonstrated the pores of about 4 nm and 7 nm in the network of the isolated GBMs by TEM of negative staining, respectively. In replica techniques, Takami et al [24] have directly demonstrated more larger pores (16 × 12 nm), whereas Kubosawa et al [50] have demonstrated the pores (20 to 25 nm) after trypsin digestion. In the present HSEM study, we demonstrated the meshwork structure composed of mainly strands about 6 nm wide and to a lesser extent granular materials. The pore sizes were about 10 nm in diameter on the epithelial surface and 10 to 14 nm in diameter on the endothelial side of the GBM, respectively (cf. Figs. 9 to 11). Similar ultrastructural features were demonstrated by another HSEM technique employed by Shirato et al [34]. They have described that the native GBM consists of the meshwork structures of 6 to 11 nm fine fibrils and scattered granular materials and proposed the presence of the topographical heterogeneity on both sides of the GBM. In our previous HSEM study [33], the meshwork structure associated with granular materials have also been observed in the isolated rat GBM by sonication method, and present results are consistent with those. After treatment with 4 M guanidine, which is widely used to extract noncollagenous components [51], granular materials were reduced and then the pore sizes of the meshworks were enlarged (unpublished data). Yurchenco and Ruben have demonstrated a polygonal network of type IV collagen (2.5 to 3 nm wide) in the amniotic basement membrane after guanidine treatment [42]. Inoue et al have proved an unmasked, irregular network of type IV collagen in Reichert's membrane [41], and thin basement membranes [40] after plasmin treatment. These results suggest that strands observed in the present HSEM study may be type IV collagen attached by some material such as laminin. We postulate that granular materials seen on the meshwork structures may be a part of noncollagenous basement membrane components and correspond to the granular background materials in the GBM seen by TEM (compare Fig. 1C and 1D with Fig. 2D). As we have not yet established the immuno-HSEM technique to clarify the chemical components of meshwork structures observed, we could not reach a conclusion on this point.

At the ultrastructural level, architectural and morphometrical discrepancies according to the methods employed may be in part accounted for by the difference in techniques to visualize macromolecular structures of the GBM. The modes of fixation, the tannin-osmium staining in HSEM technique, and the metal coating in TEM of replica techniques influence the appearance and the size of macromolecules. The effects of the mode of fixation have been discussed in detail [21, 40, 41]. They have reported that "cord" thickness is 4.8 nm in glutaraldehyde-fixed and 3.4 nm in permanganated-fixed in the rat seminiferous tubule basement membrane. Likewise, the tannin-osmium conductive staining employed in the present study, which is correspond to the metal impregnation such as uranyl acetate and lead citrate in TEM technique, is evaluated to increase the apparent size of macromolecules such as ferritin (about 35%) [52]. In the present TEM study, the fibrillar components of the GBM in glutaraldehyde-fixed specimens were slightly thinner than those measured after the tannin-osmium staining (compare Fig. 1C with 1D). Based on the results of the present TEM study and studies by Nakadera, Mitsushima and Tanaka [52], the apparent size of the strands measured in the present HSEM study might grow thicker (about 30 to 40%) and then much smaller pores (diameter < 2 nm) might be clogged.

Physiologically, the presence of the pores in the GBM has been postulated on the basis of numerous tracer studies, however, the theoretical sizes estimated vary with methods

employed as well as morphological studies [2, 3, 5]. Probably the glomerular permeability to macromolecules and plasma proteins may also be effected by molecule-filter interaction with charge [4], shape, and hemodynamic factors as well as size. The effective pore size of the GBM is considered to less than 10 nm in diameter [3, 5]. Our present data characterizing the epithelial surface of the GBM (about 10 nm in diameter) fit in with this estimate. Chang et al [2] have postulated the presence of uniform, cylindrical pores about 5 nm in the GBM. In contrast, the present data and available data suggest that a three-dimensional polygonal meshwork structure is the characteristic feature of basement membranes.

Heterogeneity of GBM

We demonstrated the presence of the ultrastructural heterogeneity in opposite sides of the GBM at high resolution of HSEM, namely, whereas the epithelial surface appeared as a densely organized meshwork structure (Fig. 3 E, F), the endothelio-mesangial surface displayed a loosely organized one (Fig. 3 A, B). The presence of the heterogeneity of the GBM has been previously described in several approaches [6, 7, 10, 18–20, 34, 53, 54]. Huang [53] has demonstrated two separate laminae densae of the GBM by TEM: one consisting of a highly cross-linked organization (epithelial lamina densa) and the other consisting of a loosely organized one (endothelial lamina densa) revealed with guanidine treatment in human kidneys. Carlson et al [54] have demonstrated the presence of the ultrastructural difference in opposite sides of the GBM after proteolytic dissection by TEM. More recent immnolocalization studies have identified that α1(IV), α2(IV), α3(IV) and α4(IV) chains are present on the endothelial side of the GBM, and novel α3(IV) and α4(IV) chains are predominant on its epithelial side [19, 20]. The heterogeneous distribution of distinct type IV collagen chains in the GBM has been also proven by biochemical studies [10, 18]. Moreover, the presence of the α5(IV) chain has been reported [13–17].

Present data may provide a structural basis for understanding the heterogeneity of the GBM proposed by morphological, immunohistochemical, biochemical, and physiological studies. These heterogeneous ultrastructures observed in both sides of the GBM may relate to (1) the dual embryonic origin of the GBM, and (2) three-dimensional expansions of the mesangial matrix via the endothelial side of the GBM. First, the GBM originates during nephrogenesis by fusion of double basement membranes beneath the vascular endothelium and the visceral epithelium, respectively. The evidence that the synthesis of additional basement membranes and joining of the new basement membrane with the GBM by splicing during glomerular developments, demonstrated by Abrahamson and Perry [55], indicates a heterogeneous distribution of distinct five type IV collagen chains in the matured GBM. Second, the three-dimensional expansion of the mesangial matrix was observed in agreement with previous morphological studies [26, 29, 56]. In the case of biochemical continuity of the GBM and the mesangial matrix, recent immunohistochemical studies have proven that α1(IV) and α2(IV) chains are predominant in the mesangial matrix and subendothelial side of the GBM [19, 20]. In the present study, we confirmed morphologically the continuity of the GBM and the mesangium on the endothelial side of the GBM at high resolution of HSEM (Fig. 3B). This looser organization observed on the endothelio-mesangial surface of the GBM may allow for penetration of macromolecules through the endothelial side as demonstrated by tracer studies of endogenous albumin and IgG [6, 7].

Acknowledgments

This research was supported in part by a Grant-in-Aid for Scientific Research from the Ministry of Education, Science and Culture and by a Research Grant for "Progressive Renal Disease" from the "Specially Selected Disease By the Ministry of Health and Welfare Research Project" of the Ministry of Health and Welfare, Japan. We thank Mr. N. Hayashi and Mr. N. Kishimoto of Central Research Laboratory, Okayama University Medical School, for their technical assistance in scanning electron microscopy. We thank Mrs. T. Hashimoto and Miss K. Nakata for their technical assistance in transmission electron microscopy.

Reprint requests to Kazue Hironaka, M.D., Third Department of Internal Medicine, Okayama University Medical School, 2-5-1 Shikata-cho, Okayama 700, Japan.

References

1. Farquhar MG, Wissing SL, Palade GE: Glomerular permeability. I. Ferritin transfer across the normal glomerular capillary wall. *J Exp Med* 113:47–66, 1961
2. Chang RLS, Deen WM, Robertson CR, Bennett CM, Glassock RJ, Brenner BM: Permselectivity of the glomerular capillary wall. *J Clin Invest* 57:1272–1286, 1976
3. Caulfield JP, Farquhar MG: The permeability of glomerular capillaries to graded dextrans. *J Cell Biol* 63:883–903, 1974
4. Kanwar YS: Biophysiology of glomerular filtration and proteinuria. *Lab Invest* 51:7–21, 1984
5. Batsford SR, Rohrbach R, Vogt A: Size restriction in the glomerular capillary wall: Importance of lamina densa. *Kidney Int* 31:710–717, 1987
6. Desjardins M, Bendayan M: Ultrastructural distribution of endogenous IgGs in the glomerular wall of control and diabetic rats. *Histochem J* 21:731–742, 1989
7. Russo PA, Bendayan M: Distribution of endogenous albumin in the glomerular wall of proteinuria patients. *Am J Pathol* 137:1481–1490, 1990
8. Wieslander J, Bygren PG, Heinegard D: Isolation of the specific glomerular basement membrane involved in Goodpasture syndrome. *Proc Natl Acad Sci USA* 81:1544–1548, 1984
9. Butkowski JR, Wieslander J, Wisdom BJ, Barr JF, Noelken ME, Hudson BG: Properties of the globular domain of type IV collagen and its relationship to the Goodpasture antigen. *J Biol Chem* 260:3739–3747, 1985
10. Langeveld JPM, Wieslander J, Timoneda J, McKinney P, Butkowski RJ, Wisdom BJ, Hudson BG: Structural heterogeneity of the noncollagenous domain of basement membrane collagen. *J Biol Chem* 263:10481–10488, 1988
11. Saus J, Wieslander J, Langeveld JPM, Quinones S, Hudson BG: Identification of the Goodpasture antigen as the α3(IV) chain of collagen IV. *J Biol Chem* 263:13374–13380, 1988
12. Gunwar S, Saus J, Noelken ME, Hudson BG: Glomerular basement membrane. Identification of a fourth chain, α4, of type IV collagen. *J Biol Chem* 265:5466–5469, 1990
13. Yoshioka K, Michael AF, Velosa J, Fish AJ: Detection of hidden nephritogenic antigen determinants in human renal and non-renal basement membranes. *Am J Pathol* 121:156–165, 1985
14. Kleppel MM, Michael AF, Fish AJ: Antibody specificity of human glomerular basement membrane type IV collagen NC1 subunits. *J Biol Chem* 261:16547–16552, 1986
15. Pihlajaniemi T, Pohjolainen ER, Myers JC: Complete primary structure of the triple-helical region and the carboxyl-terminal domain of a new type IV collagen chain, α5(IV). *J Biol Chem* 265:13758–13766, 1990
16. Hostikka SL, Eddy RL, Byers MG, Höyhtyä M, Shows TB, Tryggvason K: Identification of a distinct type IV collagen α

chain with restricted kidney distribution and assignment of its gene to the locus of chromosome-linked Alport syndrome. *Proc Natl Acad Sci USA* 87:1606–1610, 1990
17. MYERS JC, JONES TA, POHJOLAINEN ER, KADRI AS, GODDARD AD, SHEER D, SOLOMON E, PIHLAJANIEMI T: Molecular cloning of α5(IV) collagen and assignment of the gene to the region of the X chromosome containing the Alport syndrome locus. *Am J Hum Genet* 46:1024–1033, 1990
18. KLEPPEL MM, FAN WW, CHEONG H II, MICHAEL AF: Evidence for separate networks of classical and novel basement membrane collagen. *J Biol Chem* 267:4137–4142, 1992
19. DESJARDINS M, GROS F, WIESLANDER J, GUBLER MC, BENDAYAN M: Heterogeneous distribution of monomeric elements from the globular domain (NC1) of type IV collagen in renal basement membranes as revealed by high resolution quantitative immunocytochemistry. *Lab Invest* 63:637–646, 1990
20. BUTKOWSKI R, WIESLANDER J, KLEPPEL M, MICHAEL AF, FISH AJ: Basement membrane collagen in the kidney: Regional localization of novel chains related to collagen IV. *Kidney Int* 35:1195–1202, 1989
21. LAURIE GW, LEBLOND CP, INOUE S, MARTIN GR, CHUNG A: Fine structure of the glomerular basement membrane and immunolocalization of five basement membrane components to the lamina densa (basal lamina) and its extensions in both glomerular and tubules of the rat kidney. *Am J Anat* 169:463–481, 1984
22. OTA Z, MAKINO H, TAKAYA Y, OFUZI T: Molecular sieve in renal glomerular and tubular basement membranes as revealed by electron microscopy. *Renal Physiol* (Basel) 3:317–323, 1980
23. MARTINEZ-HERNANDEZ A: The basement membrane pores, in *Biology and Chemistry of Basement Membranes*, edited by KEFALIDES NA, New York, Academic Press, 1978, pp. 99–109
24. TAKAMI H, NARAMOTO A, SHIGEMATU H, OHNO S: Ultrastructure of glomerular basement membrane by quick-freeze and deep-etch methods. *Kidney Int* 39:659–664, 1991
25. CARLSON ED, KENNY MC: Preparation and histoarchitecture of ultrastructurally pure glomerular basement membrane. *Renal Physiol* 3:280–287, 1980
26. CARLSON EC, HINDS D: A topographical (SEM) analysis of acellular glomerular mesangial matrix *in situ*. *J Ultrastruct Res* 82:96–100, 1983
27. BONSIB SM: Scanning electron microscopy of acellular glomeruli in nephrotic syndrome. *Kidney Int* 27:678–684, 1985
28. WEIDNER N, LORENTZ WB: Scanning electron microscopy of the acellular glomerular and tubular basement membranes in lupus nephritis. *Am J Clin Pathol* 85:135–145, 1986
29. MAKINO H: Three-dimensional ultrastructure of rat acellular glomerulus by scanning electron microscopy. *J Electron Microsc* 37:294–304, 1988
30. NISHINURA S, MAKINO H, OTA Z: Three-dimensional ultrastructural changes of acellular glomerular basement membrane in various types of human glomerulonephritis. *Nephron* 53:9–17, 1989
31. TANAKA K, MATUI I, KURODA K, MITSUSHIMA A: A new ultrahigh resolution scanning electron microscope (UHS-T1). *Biomedical SEM* 14:23–25, 1985 (in Japanese)
32. MURAKAMI T: A metal impregnation method of biological specimen for scanning electron microscopy. *Arch Histol Jpn* 35:323–326, 1973
33. YAMASAKI Y, MAKINO H, HIRONAKA K, OTA Z: Three-dimensional architecture of rat glomerular basement membrane by ultrahigh resolution scanning electron microscopy. *Acta Medica Okayama* 44:333–335, 1990
34. SHIRATO I, TOMINO Y, KOIDE H, SAKAI T: Fine structure of the glomerular basement membrane of the rat kidney visualized by high-resolution scanning electron microscopy. *Cell Tissue Res* 266:1–10, 1991
35. KORIYAMA Y, YAMADA E, WATANABE I: "Pored-domes" of the fenestrated endotheliocyte of the glomerular and peritubular capillaries in the rodent kidney. *J Electron Microsc* 41:30–36, 1992
36. SPIRO RG: Studies on the renal glomerular basement membrane. *J Biol Chem* 242:1915–1922, 1967
37. HOUSER MJ, SHEINMAN JI, BASGEN J, STEFFES MW, MICHAEL AF: Preservation of mesangium and immunohistochemically defined antigens in glomerular basement membrane isolated by detergent extraction. *J Clin Invest* 69:1169–1175, 1982
38. COURTOY PJ, TIMPL R, FARQUHAR MG: Comparative distribution of laminin, type IV collagen, and fibronectin in the rat glomerulus. *J Histochem Cytochem* 30:874–886, 1982
39. KANWAR YS, FARQUHAR MG: Anionic sites in the glomerular basement membrane. *In vivo* and *in vitro* localization to the laminae rarae by cationic probes. *J Cell Biol* 81:137–153, 1979
40. INOUE S, LEBLOND CP: Three-dimensional network of cords: The main component of basement membranes. *Am J Anat* 181:341–358, 1988
41. INOUE S, LEBLOND CP, LAURIE GW: Ultrastructure of Reichert's membrane, a multilayered basement membrane in the parietal wall of the rat yolk sac. *J Cell Biol* 97:1524–1537, 1983
42. YURCHENCO PD, RUBEN GC: Basement membrane structure *in situ*: Evidence for lateral association in the type IV collagen network. *J Cell Biol* 105:2559–2568, 1987
43. JAFFÈ R, BENDER B, SANTAMARIA M, CHUNG AE: Segmental staining of the murine nephron by monoclonal antibodies directed against the GP-2 subunit of laminin. *Lab Invest* 51:88–96, 1984
44. MARTINEZ-HERNANDEZ A, CHUNG AE: The ultrastructural localization of two basement membrane components: Entactin and laminin in rat tissues. *J Histochem Cytochem* 32:289–298, 1984
45. GRANT DS, LEBLOND CP: Immunogold quantitation of laminin, type IV collagen, and heparan sulfate proteoglycan in a variety of basement membranes. *J Histochem Cytochem* 36:271–283, 1988
46. DESJARDINS M, BENDAYAN M: Heterogeneous distribution of type IV collagen, entactin, heparan sulfate proteoglycan, and laminin among renal basement membranes as demonstrated by quantitative immunocytochemistry. *J Histochem Cytochem* 37:885–897, 1989
47. ABRAHAMSON DR, IRWIN MH, JOHN PL, PERRY EW, ACCAVITTI MA, HECK LW, COUCHMAN JR: Selective immunoreactivities of the kidney basement membrane to monoclonal antibodies laminin: Localization of the end of the long arm and the short arm to discrete microdomains. *J Cell Biol* 109:3477–3491, 1989
48. KATZ A, FISH AJ, KLEPPEL MM, HAGEN SG, MICHAEL AF, BUTKOWSKI RJ: Renal entactin (nidogen): Isolation, characterization and tissue distribution. *Kidney Int* 40:643–652, 1991
49. BOOT-HANDFORD RP, KURKINEN M, PROCKOP DJ: Steady-state levels of mRNAs coding for the type IV collagen and laminin polypeptide chains of basement membranes exhibit marked tissue-specific stoichiometric variations in the rat. *J Biol Chem* 262:12475–12478, 1987
50. KUBOSAWA H, KONDO Y: Ultrastructural organization of the glomerular basement membrane as revealed by a deep-etch replica method. *Cell Tissue Res* 242:33–39, 1985
51. PAULSSON M, YURCHENCO PD, RUBEN GC, ENGEL J, TIMPL R: Structure of low density heparan sulfate proteoglycan isolated from a mouse tumor basement membrane. *J Mol Biol* 197:297–313, 1987
52. NAKADERA T, MITSUSHIMA A, TANAKA K: Application of high-resolution scanning electron microscopy to biological macromolecules. *J Electron Microsc* 163:43–50, 1991
53. HUANG TW: Basal lamina heterogeneity in the glomerular capillary tufts of human kidneys. *J Exp Med* 149:1450–1459, 1979
54. CARLSON EC, MEEZAN E, BRENDEL K, KENNY MC: Ultrastructural analyses of control and enzyme-treated isolated renal basement membranes. *Anat Rec* 200:421–436, 1981
55. ABRAHAMSON DR, PERRY EW: Evidence for splicing new basement membrane into old during glomerular development in newborn rat kidneys. *J Cell Biol* 103:2489–2498, 1986
56. KEANE WF, RAIJ L: Impaired mesangial clearance of macroolecules rats with chronic mesangial ferritin-antiferritin immune complex deposition. *Lab Invest* 43:500–507, 1980